

TURNING AROUND ALONG THE COSMIC WEB

Jounghun Lee¹ and Gustavo Yepes^{2,3}

ABSTRACT

A bound-violation designates a case that the turn-around radius of a bound object exceeds the upper limit put by the spherical collapse model based on the standard Λ CDM paradigm. Given that the turn-around radius of a bound object is a stochastic quantity and that the spherical model overly simplifies the true gravitational collapse which actually proceeds anisotropically along the cosmic web, the rarity of the occurrence of a bound violation may depend on the web environment. Assuming a Planck cosmology, we numerically construct the bound-zone peculiar velocity profiles along the cosmic web (filaments and sheets) around the isolated groups with virial mass $M_v \geq 3 \times 10^{13} h^{-1} M_\odot$ identified in the Small MultiDark Planck simulations and determine the radial distances at which their peculiar velocities equal the Hubble expansion speed as the turn-around radii of the groups. It is found that although the average turn-around radii of the isolated groups are well below the spherical bound-limit on all mass scales, the bound violations are not forbidden for individual groups and that the cosmic web has an effect of reducing the rarity of the occurrence of a bound violation. Explaining that the spherical bound limit on the turn-around radius in fact represents the threshold distance up to which the intervention of the external gravitational field in the bound-zone peculiar velocity profiles around the *non-isolated* groups stays negligible, we discuss the possibility of using the threshold distance scale to constrain locally the equation of state of dark energy .

Subject headings: cosmology — large scale structure of universe

¹Astronomy Program, Department of Physics and Astronomy, Seoul National University, Seoul 08826, Korea

jounghun@astro.snu.ac.kr

²Departamento de Física Teórica, Universidad Autónoma de Madrid, 28049 Madrid, Spain

³ASTRO UAM, UAM Unidad Asociada CSIC.

1. INTRODUCTION

In a Λ CDM (the cosmological constant Λ + cold dark matter) universe, a mildly overdense site which accretes masses from the surrounding with growing comoving radius will never encounter the turn-around moment since its gravity will be incapable of winning over the accelerating expansion of spacetime driven by such inert dark energy as Λ . Therefore, only those overdense sites that have already formed bound objects until the present epoch or at least turned around before the onset of the accelerating phase of spacetime can possess finite turn-around radii, defined as the effective radii of the sites at the moment when their gravitational force begins to hold down the Hubble expansion (Pavlidou & Tomaras 2014; Pavlidou et al. 2014). In other words, the standard Λ CDM cosmology generically predicts the existence of a finite upper limit on the turn-around radii of the bound objects observed in the local universe.

Pointing out that the turn-around radius of a bound object, r_t , is a well defined linear quantity, Pavlidou & Tomaras (2014) found an analytic expression for the upper limit, $r_{t,u}$, on the possible values of r_t under one simplified assumption that the gravitational collapse after the turn-around moment proceeds isotropically:

$$r_{t,u} = \left(\frac{3MG}{\Lambda c^2} \right)^{1/3}, \quad (1)$$

Strictly speaking, M in the RHS of Equation (1) denotes the mass enclosed by the turn-around radius r_t the ratio of which to virial mass M_v depends on mass scales and redshifts. Notwithstanding, Pavlidou & Tomaras (2014) suggested that the upper limit of the turn-around radius be expressed in terms of a readily measurable mass like the virial mass since the mass enclosed by r_t cannot be independently measured in practice. See Pavlidou & Tomaras (2014) for the detailed explanations. Throughout this paper, we approximate M in the RHS of Equation (1) by M_v .

Equation (1) predicts that the average turn-around radius on the mass scale M_v stays much lower than $r_{t,u}$. If a substantially large number of the objects in the local universe should be found to exhibit a bound violation having larger turn-around radii than $r_{t,u}$ given in Equation (1), then it would challenge the Λ CDM model. As mentioned in Pavlidou & Tomaras (2014), the upside of using the turn-around radii of the bound objects as a test of the Λ CDM model lies in the fact that it requires only local observables whose systematics would be better controlled unlike the standard global diagnostics which usually require to measure the growth and/or expansion history of the whole universe (see Linder 2003, 2005, and references therein).

In the conventional approach, the values of r_t of the galaxy groups and clusters observed

in the local universe have been estimated by directly measuring the distances to the surfaces of the zero radial velocities of the bound-zone galaxies (e.g., see Karachentsev et al. 2014, and references therein). However, the estimates of r_t based on this conventional method has been known to suffer from low accuracy that is imputable to notoriously large uncertainties in the measurements of the peculiar velocities of the bound-zone galaxies around the groups and clusters (see Pavlidou & Tomaras 2014). Very recently, Lee et al. (2015) proposed a new methodology to overcome the low accuracy in the estimation of r_t and applied it to a nearby galaxy group NGC 5353/4 (Tully & Trentham 2008; Tully 2015). Their methodology turned largely to the numerical claim of Falco et al. (2014) that the peculiar velocity profile in the bound zone around a massive group takes on a universal form and that the profile can be readily reconstructed from the two-dimensional spatial distributions of the bound-zone galaxies along the cosmic web.

The turn-around radius of NGC5353/4 estimated by Lee et al. (2015) with their new method was found to commit a bound violation. That is, the value of r_t of the NGC 5353/4 group has been found to exceed the upper limit $r_{t,u}$ given in Equation (1). Being cautious and conservative, Lee et al. (2015) have suggested that the robustness of the new method as well as the validity of the universal formula for the peculiar velocity profile proposed by Falco et al. (2014) should be thoroughly examined before putting a proper interpretation of their result. As clearly mentioned in Pavlidou & Tomaras (2014), the turn-around radius of an object is a stochastic quantity, varying in a broad range. Equation (1) puts the upper limit on the *average* turn-around radius on the mass scale M_v but not on all turn-around radii of individual objects with virial mass M_v . In other words, it might not be forbidden even in the Λ CDM cosmology to observe an individual object with mass M_v whose turn-around radius exceeds the spherical bound-limit. What Equation (1) truly implies is that it would be quite rare to witness a bound violation in the Λ CDM universe.

Besides, what has not been properly taken into account in the analytic derivation of $r_{t,u}$ by Pavlidou & Tomaras (2014) is the fact that the true gravitational collapse proceeds quite anisotropically (Bond & Myers 1996) which is responsible for the eventual formation of the cosmic web in the universe (Bond et al. 1996). Although Lee et al. (2015) used the same analytic formula proposed by Falco et al. (2014) to make an estimate of the turn-around radius of NGC 5353/4 along the filament, it has yet to be tested whether or not the peculiar velocity profile constructed along the cosmic web would still be validly approximated by the same formula that was obtained by taking the isotropic average over all directions. Thus, the remaining critical questions are (1) how rare occasion a bound violation is in a Λ CDM universe; and (2) how the true gravitational collapse that tends to proceed anisotropically along the cosmic web affects the rarity of the occurrence of bound violation, both of which we attempt to answer in this work.

The contents of this Paper can be summarized as follows. In Section 2 a brief review of the methodology of Lee et al. (2015) and its key assumptions are presented. In Section 3 a comprehensive numerical test of the methodology is presented and the effect of the web environment on the construction of the peculiar velocity profiles is explored. In Section 4 the estimates of the turn-around radii along the cosmic web on various mass scales are presented. In Section 5 the final results are summarized and the physical implications are discussed.

2. METHODOLOGY AND THE KEY ASSUMPTIONS: A REVIEW

Let us consider a spatial point at a distance, r , from the center of a massive group with virial radius, r_v , in a space expanding at a global rate, H_0 . From here on, the radial component of the peculiar velocity field in the direction from the halo center to the spatial point is called *the peculiar velocity at r* for short. If the distance r is included in the bound zone range of $3 \leq r/r_v \leq 8$ where the subspace expands at a lower rate than H_0 due to the net gravitational effect of the main group, the spherically averaged value of the peculiar velocity, v_p , at r is well depicted by the following universal formula with two parameters a and b (Falco et al. 2014):

$$v_p(r) = -a V_c \left(\frac{r}{r_v} \right)^{-b}, \quad (2)$$

where V_c is the magnitude of the circular velocity of the main group at its virial radius given as $V_c^2 = GM_v/r_v$ with virial mass M_v . Fitting Equation (2) to the numerical results from a high-resolution N -body simulation, Falco et al. (2014) found $a = 0.8 \pm 0.2$ and $b = 0.42 \pm 0.16$ and speculated that these best-fit values of the two parameters would be insensitive to the redshifts as well as to the mass scales.

Inspired by the existence of the universal peculiar velocity profile in the bound zone, Lee et al. (2015) suggested that the turn-around radius, r_t , of a main group be readily obtained just as the value at which the following relation is satisfied:

$$H_0 r_t = a V_c \left(\frac{r_t}{r_v} \right)^{-b}, \quad (3)$$

where the left-hand side (LHS) represents the global expansion speed at r_t and the right-hand side (RHS) is the peculiar velocity at the same radius predicted by Equation (2). Provided that the virial radius (or equivalently, virial mass) of a massive group is already known as a prior and that the two parameters in the RHS, a and b , have truly constant values of $a \sim 0.8$ and $b \sim 0.42$ as speculated by Falco et al. (2014), solving Equation (3) for r_t should allow one to estimate the turn-around radius of a given group without necessitating an accurate measurement of the peculiar velocity field in its bound zone.

Although Falco et al. (2014) showed that Equation (2) with the constant values of a and b matched well the numerically obtained peculiar velocity profiles of three different cluster-size halos, it is inconclusive whether or not the bound-zone peculiar velocity profile is truly universal since the variations of its shape with mass and redshift were reported by other numerical works (e.g., Cuesta et al. 2008; Lee 2016). To account for the possibility that the bound-zone peculiar velocity profile may not be universal, it is unavoidable to regard a and b in Equation (2) as two *varying parameters* and to determine their best-fit values by fitting Equation (2) to the bound-zone peculiar velocity profile constructed from observational data before estimating r_t .

The practical feasibility of constructing the bound-zone peculiar velocity profiles was improved by Falco et al. (2014) who showed that if the average of the peculiar velocity field was taken over the spatial points distributed along the cosmic web (filaments and sheets), $v_p(r)$ can be expressed in terms of directly measurable quantities:

$$\frac{c\Delta z}{\cos \beta} - H_0 \frac{R}{\sin \beta} = -aV_v \left(\frac{R}{\sin \beta r_v} \right)^{-b}. \quad (4)$$

Here Δz represents the difference in redshifts between the main group and a bound-zone object, R is the projected distance of the bound-zone object from the group center in the plane of sky, and β is the inclination angle between the direction of the cosmic web and the line-of-sight, which are all directly measurable without making any specific assumption about the background cosmology. Lee et al. (2015) determined the values of a and b via adjusting the RHS to the LHS in Equation (4) that can be also directly computed from the observables. Applying this method to the bound zone of the NGC 5353/4 group around which a narrow filamentary structure was detected (S.Kim in private communication), Lee et al. (2015) pulled it off to estimate its turn-around radius.

3. EFFECT OF THE COSMIC WEB ON THE VELOCITY PROFILE

The halo catalog from the Small MultiDark Planck simulation (SMDPL) at $z = 0$ is utilized to perform our numerical investigation. As a part of MultiDark and Bolshoi Project (Klypin et al. 2016), SMDPL was conducted with 3840^3 particles of individual mass $9.63 \times 10^7 h^{-1} M_\odot$ in a periodic box of a volume $400^3 h^{-3} \text{Mpc}^3$ (Klypin et al. 2016) for a Planck cosmology, i.e., a flat Λ CDM cosmology with $h = 0.68$, $\Omega_\Lambda = 0.69$, $\Omega_m = 0.31$, $\Omega_b = 0.048$, $\sigma_8 = 0.82$, $n_s = 0.96$ (Planck Collaboration et al. XVI. 2014). The SMDPL halo catalog at $z = 0$ provides information on the comoving position (\mathbf{x}), peculiar velocity (\mathbf{v}), virial radius and mass (r_v and M_v) of each dark matter halo identified by applying the Rockstar halo finder to the phase space distributions of the particles (Behroozi et al. 2013).

The massive Rockstar halos with virial mass $M_v \geq 3 \times 10^{13} h^{-1} M_\odot$ are selected from the SMDPL catalog as the *main groups* whose bound-zone peculiar velocity profile and turn-around radii are to be estimated in the current work. The lower-mass halos $M_v < 3 \times 10^{13} h^{-1} M_\odot$ are excluded from the sample of the main groups since the number of the neighbor halos in their bound zones is not large enough to construct the peculiar velocity profiles. A total of 8476 halos in the SMDPL catalog at $z = 0$ are found to be above the imposed mass cut-off and thus included in our sample of the main groups. Throughout this analysis we focus only on the present epoch ($z = 0$) to match the real observations since the prior information in the virial radius and mass of the main groups required for our analysis is available with high accuracy only for the case of the objects located in the nearby universe.

The region inside a spherical shell surrounding each main group with inner (outer) radius of $3r_v$ ($8r_v$) from the group center is designated as its bound zone. To construct the peculiar velocity profile from the halos located in the bound zone around each main group, we consider only those well resolved halos composed of 500 or more particles, which should help us avoid numerical flukes. Basically, we search for those halos with $M_v \geq 5 \times 10^{10} h^{-1} M_\odot$ in the bound zone of each main group and then measure their separation distance vectors, \mathbf{r} , from the group center. The relative peculiar velocity of each bound-zone halo, v_p is determined as $v_p = (\mathbf{v}_h - \mathbf{v}_g) \cdot \mathbf{r} / |\mathbf{r}|$ where \mathbf{v}_h and \mathbf{v}_g are the peculiar velocities of a bound-zone halo and a main group, respectively.

To construct the peculiar velocity profile from the bound zone halos distributed along all directions, we first rescale the separation distance and the peculiar velocity of each bound-zone halo as $\tilde{r} = r/r_v$ and $\tilde{v}_p = v_p/V_c$, respectively, where r_v and V_c are the virial radius and circular velocity of its main group, respectively. Dividing the range of \tilde{r} into ten short intervals, we calculate the mean value of the rescaled peculiar velocity at each \tilde{r} -interval. Taking the ensemble average of the mean peculiar velocity at each \tilde{r} -interval over all of the selected main groups, we numerically construct $\tilde{v}_p(\tilde{r})$. The errors associated with $\tilde{v}_p(\tilde{r})$ is also calculated as one standard deviation in the measurement of the ensemble average at each \tilde{r} -interval. We finally fit the resulting numerical data points, $\tilde{v}_p(\tilde{r})$, to Equation (2) by adjusting the values of the two parameters, a and b , with the help of the maximum-likelihood method (Wall & Jenkins 2012). The best-fit values are determined to be $a = 0.74 \pm 0.01$ and $b = 0.31 \pm 0.01$ where the marginalized error in the determination of each parameter is obtained by treating the other parameter as a nuisance one.

In Figure 1, the black filled circles represent the numerical result of \tilde{v}_p with errors while the red solid line displays the analytic formula, Equation (2), with the best-fit values $a = 0.74$ and $b = 0.31$. The blue dotted line is the analytic formula with the two parameters set at the original values of $a = 0.8$ and $b = 0.42$ given by Falco et al. (2014). Figure 1 clearly reveals

that although the best-fit values of a and b are determined to be different from the original values given in Falco et al. (2014), Equation (2) with the best-fit parameters successfully describes the behavior of the bound-zone peculiar velocity profile, which is consistent with the result of Lee (2016).

Now, we want to explore how the best-fit values of a and b change when the construction of the mean peculiar velocity profile in the bound zone is done along the cosmic web. Three dimensional spatial distributions of the bound-zone halos around a main group randomly selected from our sample is illustrated in Figure 2, which gives a glimpse of a specific direction along which the number density of the bound-zone halos is conspicuously high, corresponding to the direction of a bound-zone filament. As expected, the bound-zone halos are not distributed isotropically.

To construct the peculiar velocity profile of each main group along the bound-zone sheet, we first measure the cosines of the polar angles of the position vectors, \mathbf{r} , of the bound-zone objects from the center of each main group. Then, we divide the volume into ten slices through binning the values of $\cos\theta$ and count the number of the bound-zone objects whose values of $\cos\theta$ belong to each bin. Locating the slice to which the largest number of the bound-zone objects belong and designating it as the bound-zone sheet, we include only those objects belonging to the bound-zone sheet to calculate the mean rescaled peculiar velocity profile for each main group. Taking the ensemble average of the profiles over all of the main groups, we finally construct the peculiar velocity profile from the bound-zone halos distributed along the bound-zone sheet, which is shown as the black filled circles in Figure 3.

As can be seen, in the large \tilde{r} -section ($\tilde{r} > 5.5$), the magnitude of $\tilde{v}_p(\tilde{r})$ does not monotonically decrease with \tilde{r} unlike the case that the construction of $\tilde{v}_p(\tilde{r})$ is performed from the bound-zone halos distributed along all directions (see Figure 1). Rather, it has a minimum value at $\tilde{r} \sim 5.5$ and becomes almost constant in the range of $\tilde{r} \geq 5.5$. Fitting Equation (2) only to those numerical data points in the range of $\tilde{r} \leq 5.5$ yields $a = 0.69 \pm 0.01$ and $b = 0.24 \pm 0.01$. The red solid line in Figure 3 corresponds to the analytic model with these best-fit parameters. In the restricted range of $\tilde{r} \leq 5.5$, the best-fit formula still works well, as can be seen.

For the construction of \tilde{v}_p along the bound-zone filament, we also measure the azimuthal angles (ϕ) of the position vectors, \mathbf{r} , of the bound-zone objects around each main group. The bound-zone volume of each main group is first divided into 100 conic subvolumes through simultaneously binning the values of θ and ϕ . Counting the number of the bound-zone halos belonging to each subvolume, we locate the conic subvolume which contains the maximum number of the bound-zone halos and designate it as the bound-zone filament. Using only

those bound-zone halos belonging to the bound-zone filaments, we construct the average peculiar velocity profile, which is shown as black filled circles in Figure 4. Note that the magnitude of \tilde{v}_p touches its minimum value at $\tilde{r} \sim 5.5$ and changes its trend, increasing with \tilde{r} in the range of $\tilde{r} > 5.5$. Equation (2) fitted only to those numerical data points in the range of $\tilde{r} \leq 5.5$ is shown as red solid line in Figure 4, where the two parameters are set at their best-fit values found to be $a = 0.55 \pm 0.01$ and $b = 0.20 \pm 0.01$.

The distinct behaviors of \tilde{v}_p in the range of $\tilde{r} > 5.5$ revealed by Figures 3 and 4 clearly demonstrate that Equation (2) with constant values of a and b fails to describe the peculiar velocity profiles constructed along the bound-zone sheets and filaments. Our explanation for this result is as follows. In the bound-zone around a main group, the halos would be affected not only by the gravity of the main group but also by that of the neighbor groups located outside the bound zone. When the peculiar velocity profile is constructed by taking the average over all directions, the gravitational forces from the neighbor groups would be cancelled out and thus have no net effect on the behaviors of the bound-zone peculiar velocity profile. However, when the construction of the peculiar velocity profile is made along the sheets and filaments, the gravitational forces from the neighbor halos no longer average out to zero but have non-zero net effect of flattening or increasing the magnitude of the peculiar velocities of the bound-zone halos at the distances larger than some threshold distance.

The comparison between the two results in Figures 3 and 4 indicates that when the bound-zone peculiar velocity profile is constructed along one dimensional filament, the profile in the range of $\tilde{r} > 5.5$ becomes more severely contaminated by the gravitational influences of the neighbor groups outside the bound zone. This result is in line with the recent finding of Svensmark et al. (2015) that the gravitational forces of the surrounding large-scale structures quantified by the two halo terms in the density correlation function (Ma & Fry 2000; Hayashi & White 2008) have the strongest effect on the peculiar velocities of the galaxies that fall into the clusters along the filaments.

To see the trend of \tilde{v}_p with the variation of the range of M_v , we also divide the values of M_v into three intervals and reconstruct \tilde{v}_p by using only those main groups whose masses belong to each M_v -interval. Figure 5 shows how differently the peculiar velocity profiles constructed along all directions and along the cosmic web behave for three cases of the M_v bins. The best-fit values of a and b as well as the numbers of the main groups for each case are listed in Table 1. As can be seen, the best-fit amplitude and slope decrease as the mass scales of the main groups decrease (see, also Cuesta et al. 2008). For the case of the most massive groups with $M_v \geq 10^{14} h^{-1} M_\odot$, the amplitude and slope of the bound-zone peculiar velocity profile constructed along all directions have the best-fit values of $a = 0.88 \pm 0.02$ and $b = 0.43 \pm 0.01$, which agree well with the original values determined by Falco et al. (2014).

Whereas, the other two cases of the lower-mass groups yield substantially lower slopes and amplitudes than the original values, which implies that the lower masses are less central since the energy consideration requires the slope to be close to $b \sim 0.5$ for the central masses.

Figure 5 also displays in the middle and left panels how the shapes of the peculiar velocity profiles constructed along the cosmic web differ between the M_v -bins and Table 1 lists the best-fit values of a and b for each case that the construction of \tilde{v}_p are made along the cosmic web. Note that the less massive a main group is, the more rapidly the magnitude of its bound-zone peculiar velocity profile constructed along filaments increases with distance in the section of $\tilde{r} > 5.5$. The same logic provided in the above can also explain this result: The gravitational forces of the neighbor groups outside the bound zone should have stronger influences on the bound zones around the lower mass groups.

It is worth noting that the threshold value of the rescaled distances, say \tilde{r}_c , at which the monotonic decreases of the magnitudes of the peculiar velocity profiles constructed along the cosmic web come to a halt seem to be constant $r_c \approx 5.5$. The threshold value of \tilde{r}_c represents the maximum rescaled distance up to which the gravitational effect of the neighbor groups outside the bound zone on \tilde{v}_p is negligible. We make a serendipitous discovery that the threshold rescaled distance, \tilde{r}_c , coincides with the value of the following ratio:

$$\frac{r_{t,u}}{r_v} = \left(\frac{3M_v G}{\Lambda c^2} \right)^{1/3} \times \frac{1}{r_v} \quad (5)$$

$$= \left[\frac{4\pi \rho_c \Delta_v G}{\Lambda c^2} \right]^{1/3} \approx 5.43 \quad (6)$$

Here, we employ the relation of $M_v = (4\pi/3)\Delta_v \rho_c r_v^3$ where ρ_c is the critical density at the present epoch and $\Delta_v \sim 100$ is the ratio of the mass density inside r_v to ρ_c (Falco et al. 2014). The dotted blue lines shown in Figures 3-5 correspond to this ratio, $r_{t,u}/r_v$.

It may be worth discussing here why we did not follow the conventional scheme to identify the sheets and filaments in the bound zones around the main groups. The Lagrangian perturbation theory describes that the sheets (filaments) form when the gravitational collapse proceeds anisotropically along the major (major and intermediate) principal axes of the deformation tensors calculated as the second derivatives of the perturbation potentials (Zel'dovich 1970). Accordingly, the sheets (filaments) have been conventionally identified as the regions where the local tidal shear tensors have one (two) positive and two (one) negative eigenvalues (Hahn et al. 2007).

If we identified the sheets and filaments by using the conventional scheme, however, Equation (4) would not be applicable since the success of Equation (4) requires all of the bound-zone objects belonging to a sheet (or a filament) to possess the same inclination

angles or at least to have the angles constrained in the small interval $[\cos \beta, \cos \beta + d \cos \beta]$. In other words, Equation (4) is applicable only for the case that a bound-zone sheet (filament) possesses a flat plane-like (straight line-like) shape. Our scheme is deliberately devised to ensure that the identified sheets and filament have the required shapes.

4. TURN-AROUND RADII OF THE ISOLATED GROUPS

In this Section, we are going to estimate the turn-around radii of the main groups with the help of the methodology of Lee et al. (2015) based on Equation (3). But, before embarking on the estimates of the turn-around radii, let us appreciate the implication of the results obtained in Section 3 that the bound-zone peculiar velocity profiles constructed along the cosmic web can be contaminated by the gravitational influence of its neighbor groups with comparable masses located outside the bound zone. The bottom line of Section 3 is that Equations (2) and (4) fail to describe the bound-zone peculiar velocity profiles constructed along the cosmic web. Given that the validity of Equations (2) and (4) is a key to the practical success of the methodology of Lee et al. (2015), it should be necessary to sort out those main groups whose peculiar velocity profiles are not severely contaminated by the gravitational field outside the bound zone.

We suspect that for the case of *isolated* groups which have no neighbor groups with comparable masses in the regions near to the bound zone, the contamination of the peculiar velocity profiles due to the gravitational field outside the bound-zone may be attenuated to the negligible level. For each selected main group with $M_v \geq 3 \times 10^{13} h^{-1} M_\odot$, we search for its nearest neighbor group and measured the distance, d_s , between them. Then, those groups which satisfy $d_s \geq d_c = 15r_v$ are identified as the isolated main groups. Following the same procedures described in Section 3, we construct the bound-zone peculiar velocity profiles averaged over a total of 1540 isolated main groups. Figure 6 shows the same as Figure 1 but for the case of the isolated main groups. The best-fit parameters for this case are found to be $a = 1.35 \pm 0.03$ and $b = 0.86 \pm 0.02$. As can be seen, the magnitude of the bound-zone peculiar velocity profile averaged over the isolated main groups decreases much more rapidly with \tilde{r} than that averaged over all main groups shown in Figure 1.

Figures 7 and 8 show the same as Figures 3 and 4 but for the cases of the isolated main groups, respectively. The best-fit values are found to be $a = 1.21 \pm 0.22$ and $b = 0.82 \pm 0.10$ ($a = 1.08 \pm 0.38$ and $b = 0.82 \pm 0.21$) for the case of $\tilde{v}_p(\tilde{r})$ constructed along the bound-zone sheets (filaments) around the isolated main groups. It is interesting to note that for the case of the isolated main groups, the magnitudes of \tilde{v}_p constructed along the cosmic web decrease monotonically in the whole bound zone range $3 \leq r/r_v \leq 8$ just as \tilde{v}_p constructed via

isotropic average. This result indicates that the contamination caused by the gravitational influences of the neighbor groups on the bound-zone peculiar velocity profiles vanishes for the cases of the isolated main groups, as we have anticipated. We have tested the robustness of this result against the variation of d_c and that only when $d_c \geq 15r_v$, the profile $|\tilde{v}_p|$ shows monotonic decrease with \tilde{r} in the whole range of \tilde{r} .

Figure 9 and Table 2 show the same as Figure 5 and Table 1 but for the case of the isolated main groups, respectively. It is important to note that for the cases of the isolated main groups the bound-zone peculiar velocity profiles do not show strong dependence on the mass scale M_v , although the best-fit values of a and b suffer from large errors due to the small-number statistics (especially in the large- M_v bin). The results shown in Figures 6-9 indicate that the analytic formula, Equation (2), with fixed values of a and b can reliably describe the peculiar velocity profile in the whole bound zone range only when the condition of isolation is imposed on the selection of the main groups.

Now, we are ready to estimate the turn-around radii of the isolated main groups by following the algorithm of Lee et al. (2015). First, we construct the peculiar velocity profile of each individual isolated main group and determine the best-fit values of a and b by fitting Equation (2) to each individually constructed peculiar velocity profile. Putting the best-values of a and b into Equation (3), we estimate the turn radius r_t of each individual isolated main group. Then, we divide the range of M_v into 15 bins and take the ensemble average of r_t over the isolated main groups whose virial masses belong to each M_v -bin. The one standard deviation scatter around the average is also calculated at each M_v -bin as $\sigma = (N_{\text{iso}}^{-1} \sum_{\alpha} \Delta r_{t,\alpha}^2)^{1/2}$ where N_{iso} is the number of the isolated main groups belonging to each M_v -bin and $\Delta r_{t,\alpha}$ represents the difference of the turn-around radius of the α -th main group from the ensemble average. The errors associated with the calculation of the ensemble average is also computed as $\sigma/\sqrt{N_{\text{iso}} - 1}$.

The turn-around radii r_t , estimated by the algorithm of Lee et al. (2015) is plotted versus the virial masses M_v of the isolated main groups as the black filled circles with errors in Figure 10. The red solid line is the spherical bound limit, $r_{t,u}$, given in Equation (1) predicted by the Planck cosmology. The blue dotted line is the one standard deviation scatter σ around the average values of r_t . This result clearly reveals that the spherical bound limit (red solid line) is much higher than the estimated turn-around radii in the whole mass range, implying that a bound- violation (i.e., an event of $r_t \geq r_{t,u}$) seldom occurs in the Planck universe. Note that a bound violation is relatively less rare on the low mass scale ($M_v \leq 5 \times 10^{13} h^{-1} M_{\odot}$), which can be attributed to the fact that the spherical symmetry of the gravitational collapse process breaks down more severely on the low mass scales (Bernardeau 1994).

The green solid line in Figure 10 represents the theoretical turn-around radius as a function of M_v evaluated by solving Equation (3) whose two parameters are set at the best-fit values of $a = 1.35$ and $b = 0.86$ determined from the average (not individual) peculiar velocity profile (see Figure 10). While the black filled circles with errors have been obtained by applying the method of Lee et al. (2015) to the bound-zone peculiar velocity profiles of the individual isolated groups, the green solid line has been theoretically evaluated by applying the method of Lee et al. (2015) to the mean bound-zone peculiar velocity profile averaged over all of the isolated groups. The good agreement between the black filled circles and the green solid line indicates implies the robustness and solidity of the algorithm of Lee et al. (2015) for the estimation of the turn-around radii.

Now, we would like to estimate r_t of the isolated main groups along the cosmic web. Basically, we repeat the same procedure for the estimation of $r_t(M_v)$ as described in the above but by using the individual peculiar velocity profiles \tilde{v}_p constructed along the sheets and the filaments. Figures 11 and 12 show the same as Figure 10 but for the case that the turn-around radii of the individual isolated main groups are estimated along the sheets and the filaments, respectively. To plot the green solid line in Figure 11 (Figure 12) the method of Lee et al. (2015) has been applied to the mean peculiar velocity profile shown in Figure 7 (Figure 8). As can be seen, the ensemble averages of the turn-around radii estimated along the cosmic web are still lower than the spherical upper limit in the whole mass range.

The comparison of Figures 11 and 12 with Figure 10 reveals that the values of r_t estimated along the cosmic web vary in a wider range and that the spherical bound limit (red solid line) is placed within one standard deviation scatter from the ensemble average. In other words, if the turn-around radii of the individual isolated main groups are estimated along the cosmic web, it will be less rare to witness the bound violations even in a Λ CDM universe. Hence, an observation of a single bound violation of an individual object would not challenge the standard model. Only if the spherical bound limit is found to be violated by the *average* value of the turn-around radius rather than by the individual ones, it should be regarded as an anomaly.

5. SUMMARY AND DISCUSSION

We have numerically estimated the turn-around radii r_t of the massive groups with virial mass $M_v \geq 3 \times 10^{13} h^{-1} M_\odot$ identified in the SMDPL (Klypin et al. 2016; Behroozi et al. 2013) by constructing the peculiar velocity profiles of the bound-zone halos with $M_v \geq 5 \times 10^{10} h^{-1} M_\odot$ around the groups. The shapes and behaviors of the peculiar velocity profiles have been found to vary with the directions along which the constructions were made. When

the bound-zone halos distributed along all directions are used for the constructions, the magnitudes of the resulting peculiar velocity profiles monotonically decrease with distance, being well approximated by the simple formula of Falco et al. (2014) with two characteristic parameters.

However, when only those bound-zone halos distributed along some confined directions around the groups are used for the constructions, the resulting peculiar velocity profiles exhibit distinct features: Instead of monotonically decreasing with distance, the magnitudes of the profiles reach the minimum values at some critical distances r_c and remain constant (show increment) with distance after r_c when the constructions of the profiles are made from those bound-zone halos distributed along the sheets (filaments). Explaining that this distinctly unique behaviors of the bound-zone peculiar velocity profiles constructed along the sheets and the filaments should originate from the external gravitational effect of the neighbor massive groups, we have imposed the condition of isolation on the selection of the main groups to avoid any contamination in the estimates of their turn-around radii due to the external gravity. As anticipated, it has been shown that the bound-zone peculiar velocity profiles around the isolated main groups exhibit monotonic decrement with distance, even when the profiles are constructed along the sheets and the filaments.

Finally, the average turn-around radii of the isolated main groups have been estimated from the bound-zone peculiar velocity profiles with the help of the algorithm developed by Lee et al. (2015) and found to be well below the spherical bound limit predicted by the Λ CDM cosmology in the whole mass range. We have also quantitatively shown that it is quite rare but not forbidden for individual groups to violate the bound limit especially on the relatively low-mass scale $\leq 5 \times 10^{13} h^{-1} M_\odot$ and that the rarity of the bound-violations diminishes when the turn-around radii are estimated along the cosmic web. Given our result, it has been suspected that the bound-violation of NGC 5353/4 group reported by Lee et al. (2015) may not be interpreted as a counter-evidence against the Λ CDM model at the moment.

It is worth discussing our serendipitous discovery of the coincidence between r_c and $r_{t,u}$ for the case of the non-isolated main groups. When the bound-zone peculiar velocity profiles are constructed along the filaments around the *non-isolated* main groups, the threshold distances, r_c , at which the magnitudes of the bound-zone peculiar velocities touch their minimum values coincide with the spherical upper limit, $r_{t,u}$, at all mass scales. Given that the spherical upper limit, $r_{t,u}$ is a direct indicator of the amount of Λ as shown in Equation (1), our result hints at the possibility of using r_c/r_v as another local test of the Λ CDM cosmology. Constructing the average bound-zone peculiar velocity profile along the filaments around the non-isolated massive groups from the direct observables with the help of Equation

(4) and locating where the magnitude of the average bound-zone peculiar velocity profile reaches the minimum value, we can determine r_c/r_v . Then, equating it to the theoretical constant given in Equation (5), we can estimate the amount of Λ . It would also allow us to constrain the equation of state of dark energy since the value of the spherical upper limit changes if the equation of state of dark energy deviates from -1 (Pavlidou et al. 2014). To make a robust estimate of r_c from the average bound-zone peculiar velocity profile from observations, it will be definitely necessary to use a large sample of the massive groups observed in the local universe, which is the direction of our future work.

We are very grateful to our anonymous referee for very useful comments which helped us improve the original manuscript. This work was initiated during the workshop on "Near Field Cosmology 2016" held at the Obergurgl University Centre in Tyrol, Austria from March 29 - April 3, 2016. We thank Stefan Gottlöber and the other organizers of the workshop for making stimulating discussions among the participants possible during the workshop. This study made use of data from the CosmoSim database (<http://www.cosmosim.org/>), hosted and maintained by the Leibniz-Institute for Astrophysics Potsdam (AIP). The MultiDark-Planck (MDPL) and the BigMD simulation suite have been performed on the Supermuc supercomputer at LRZ using time granted by PRACE. J.L. acknowledges the support of the Basic Science Research Program through the NRF of Korea funded by the Ministry of Education (NO. 2013004372). J.L. was also partially supported by a research grant from the National Research Foundation (NRF) of Korea to the Center for Galaxy Evolution Research (NO. 2010-0027910). G.Y. thanks MINECO/FEDER for financial support under research grants AYA2015-63810-P and AYA2012-31101.

REFERENCES

- Behroozi, P. S., Wechsler, R. H., & Wu, H.-Y. 2013, *ApJ*, 762, 109
- Behroozi, P. S., Wechsler, R. H., Wu, H.-Y., et al. 2013, *ApJ*, 763, 18
- Bernardeau, F. 1994, *ApJ*, 427, 51
- Bond, J. R., & Myers, S. T. 1996, *ApJS*, 103, 1
- Bond, J. R., Kofman, L., & Pogosyan, D. 1996, *Nature*, 380, 603
- Boylan-Kolchin, M., Springel, V., White, S. D. M., Jenkins, A., & Lemson, G. 2009, *MNRAS*, 398, 1150
- Cuesta, A. J., Prada, F., Klypin, A., & Moles, M. 2008, *MNRAS*, 389, 385
- Falco, M., Hansen, S. H., Wojtak, R., et al. 2014, *MNRAS*, 442, 1887
- Faraoni, V. 2016, *Physics of the Dark Universe*, 11, 11
- Hahn, O., Porciani, C., Carollo, C. M., & Dekel, A. 2007, *MNRAS*, 375, 489
- Hayashi, E., & White, S. D. M. 2008, *MNRAS*, 388, 2
- Karachentsev, I. D., Tully, R. B., Wu, P.-F., Shaya, E. J., & Dolphin, A. E. 2014, *ApJ*, 782, 4
- Klypin, A., Yepes, G., Gottlöber, S., Prada, F., & Heß, S. 2016, *MNRAS*, 457, 4340
- Lee, J., Kim, S., & Rey, S.-C. 2015, *ApJ*, 815, 43
- Lee, J. 2016, *arXiv:1603.06672*
- Linder, E. 2003, *Phys. Rev. Lett.*, 90, 091301
- Linder, E. V. 2005, *Phys. Rev. D*, 72, 043529
- Ma, C.-P., & Fry, J. N. 2000, *ApJ*, 543, 503
- Pavlidou, V., Tetradis, N., & Tomaras, T. N. 2014, *JCAP*, 5, 017
- Pavlidou, V., & Tomaras, T. N. 2014, *JCAP*, 9, 020
- Planck Collaboration, Ade, P. A. R., Aghanim, N., et al. 2014, *A&A*, 571, A16
- Svensmark, J., Wojtak, R., & Hansen, S. H. 2015, *MNRAS*, 448, 1644

Tully, R. B., & Trentham, N. 2008, *AJ*, 135, 1488

Tully, R. B. 2015, *AJ*, 149, 54

Wall, J. V., & Jenkins, C. R. 2012, *Practical Statistics for Astronomers*, (Cambridge, UK: Cambridge University Press)

Zel’dovich, Y. B. 1970, *A&A*, 5, 84

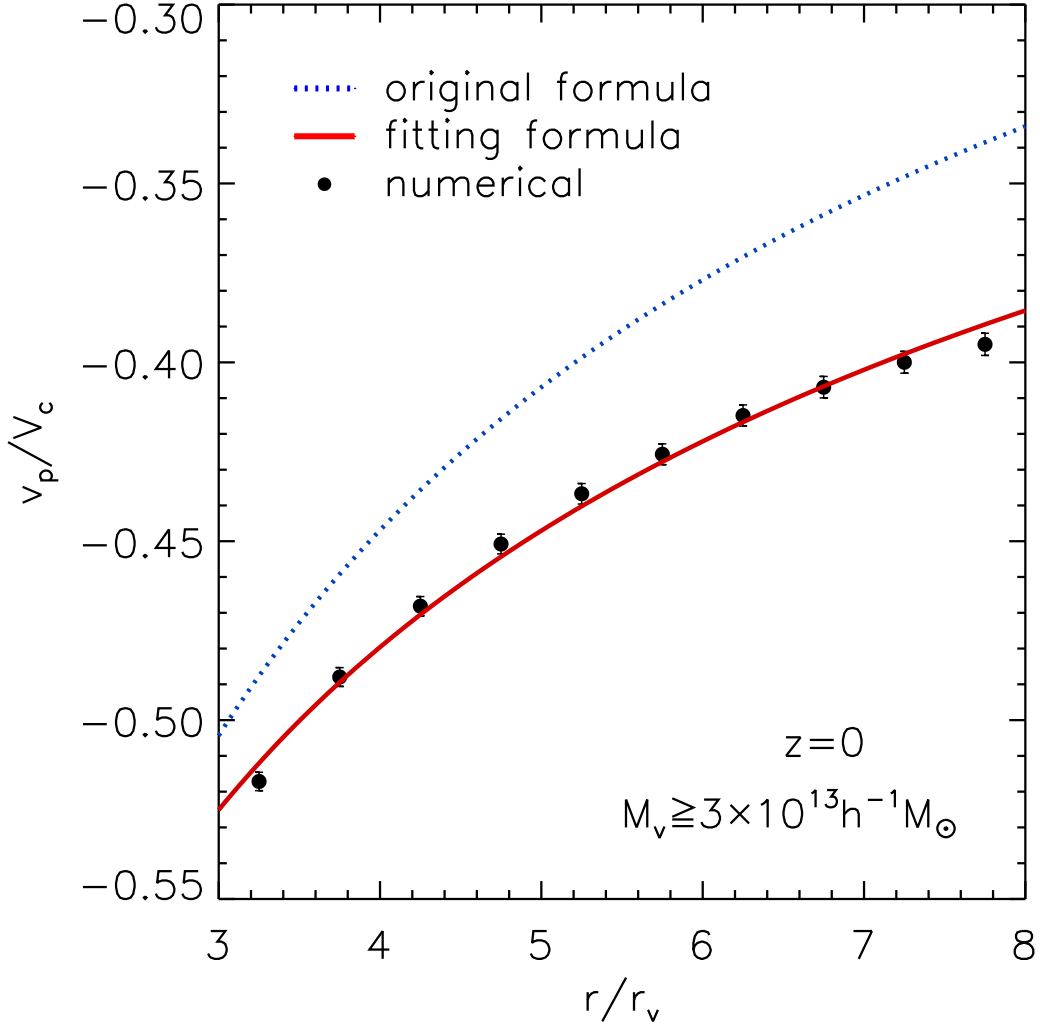


Fig. 1.— Average peculiar velocity profile of the dark matter halos located in the bound zone around the massive central halos with virial mass $M_v \geq 3 \times 10^{13} h^{-1} M_\odot$ at $z = 0$. The black filled circles with errors represent the numerical results from the Multi-Dark simulations and the red solid line represents the analytic formula with the best-fit parameters. The blue dotted lines corresponds to the original formula derived by Falco et al. (2014).

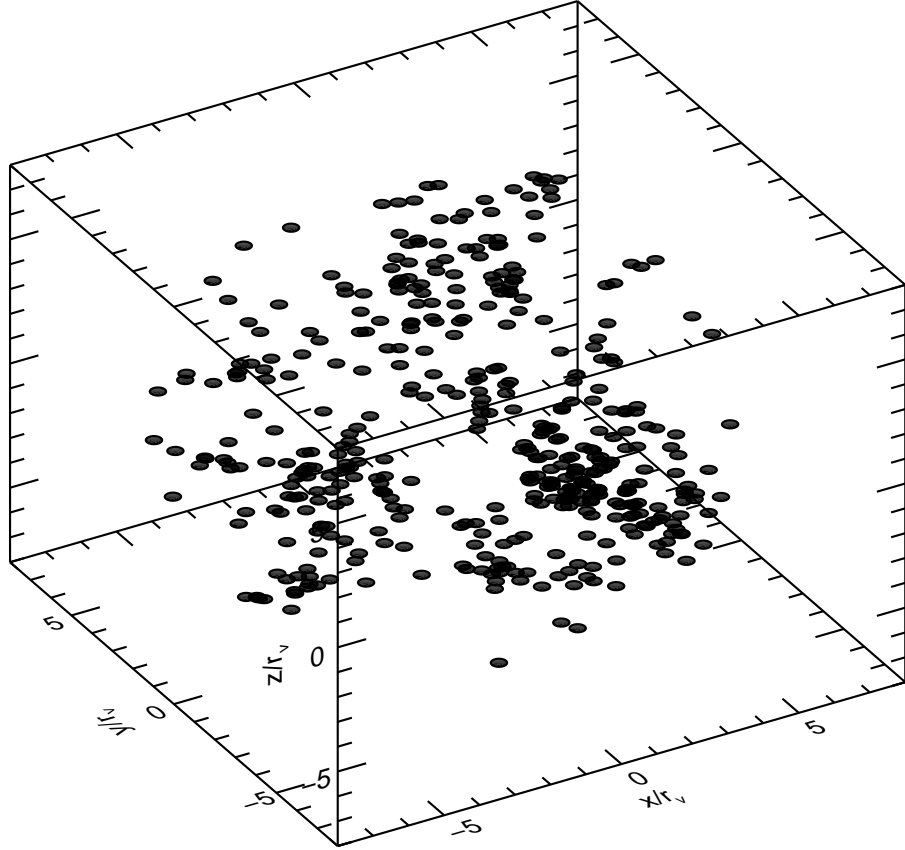


Fig. 2.— Example of three dimensional spatial distributions of the bound-zone halos around a massive central halo resolved in the Multi-dark simulation at $z = 0$.

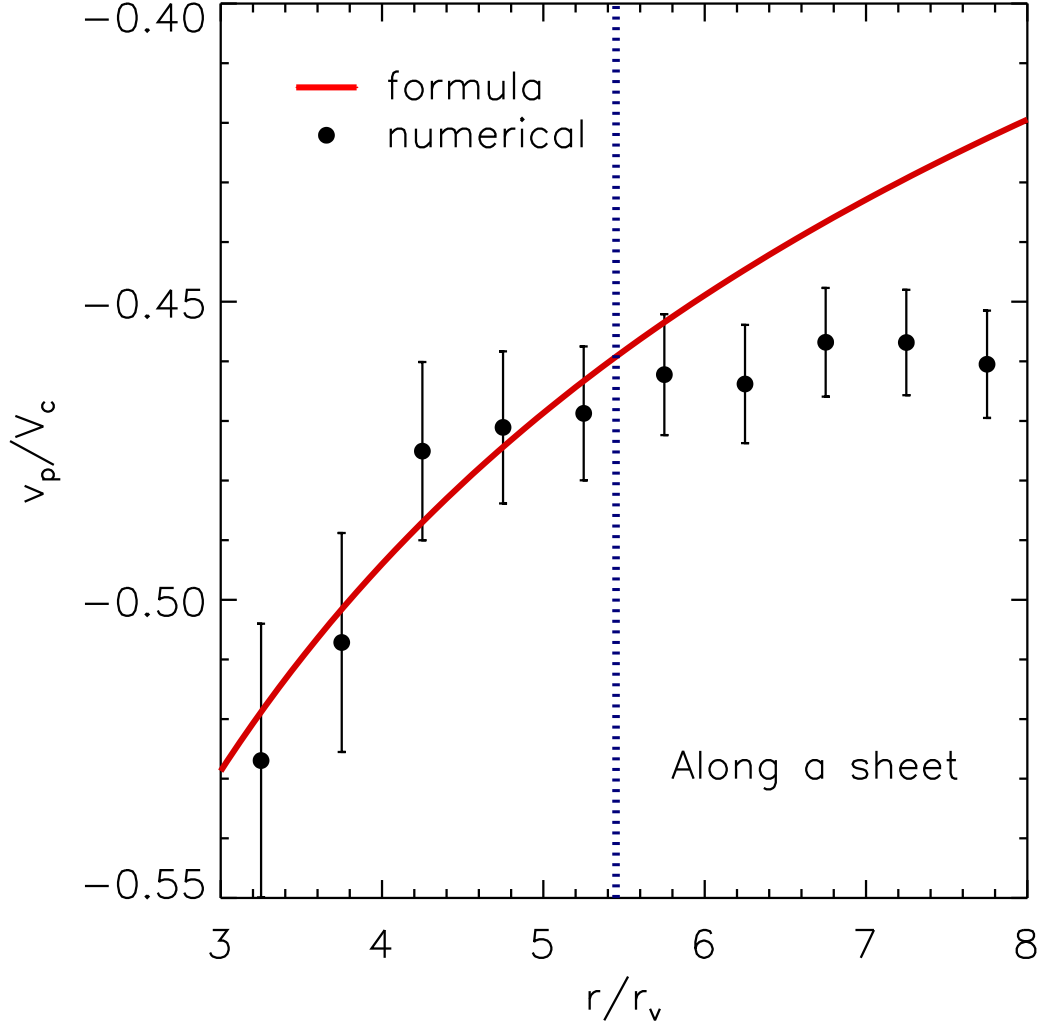


Fig. 3.— Average peculiar velocity profile constructed along the bound-zone sheet. The black filled circles with errors represent the numerical results from the Small MultiDark Planck simulations (Klypin et al. 2016) and the red solid line represents the fitting formula. The blue dotted line corresponds to the constant ratio of the bound-limit to the virial radius that is predicted to be a constant value in the Planck cosmology.

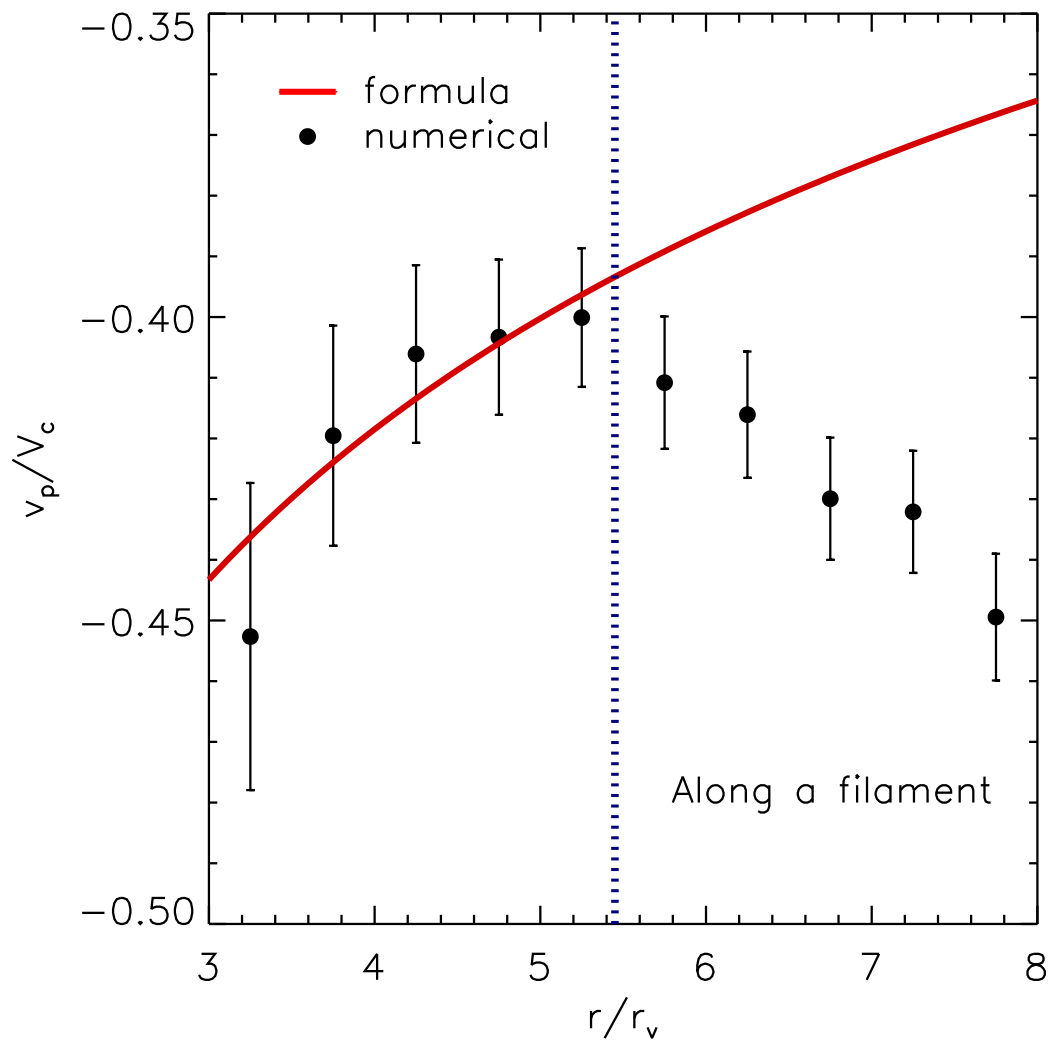


Fig. 4.— Same as Figure 3 but for the case that the average peculiar velocity profile is constructed along the bound-zone filaments.

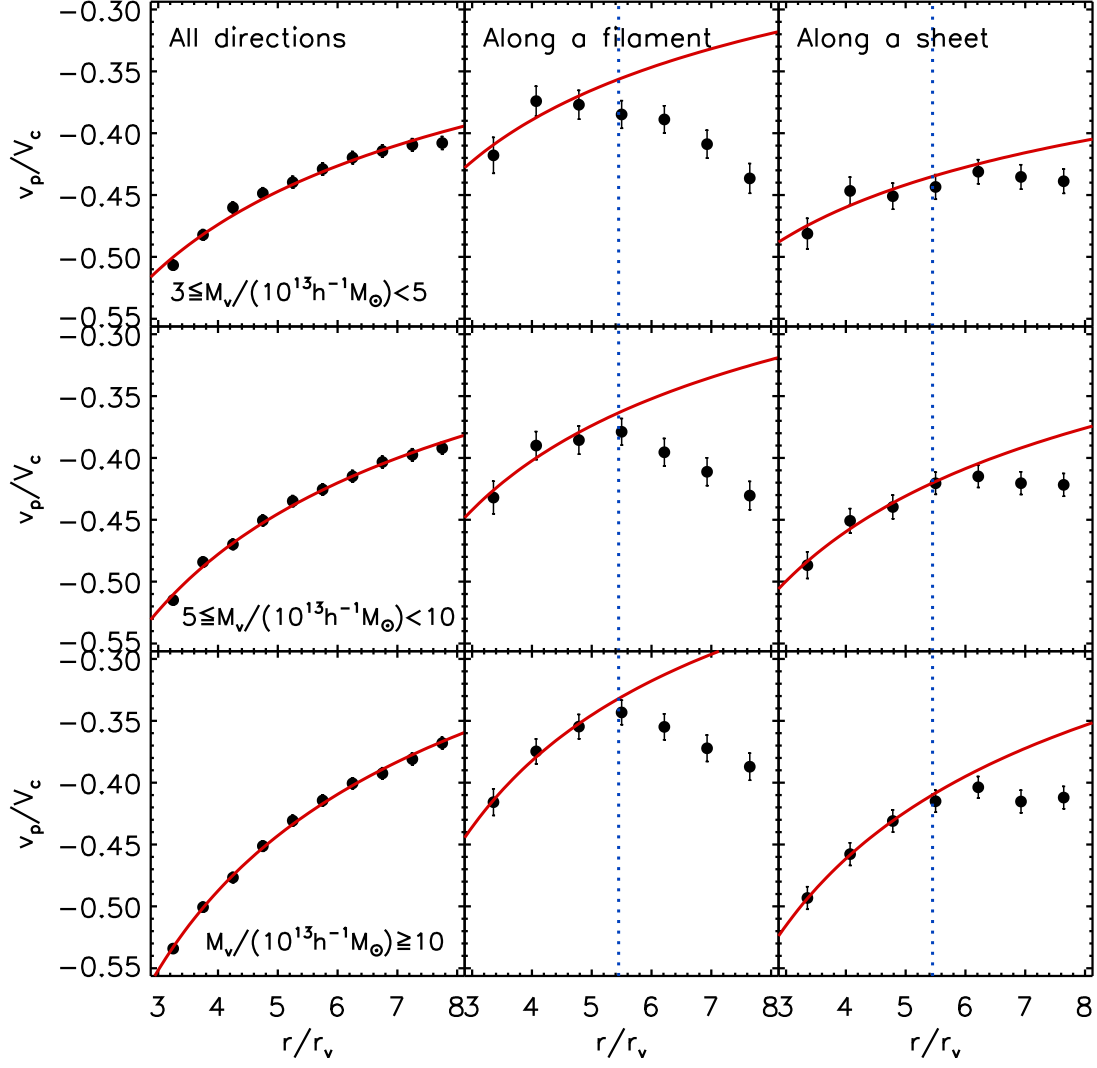


Fig. 5.— Dependence of the average peculiar velocity profiles on the mass range.

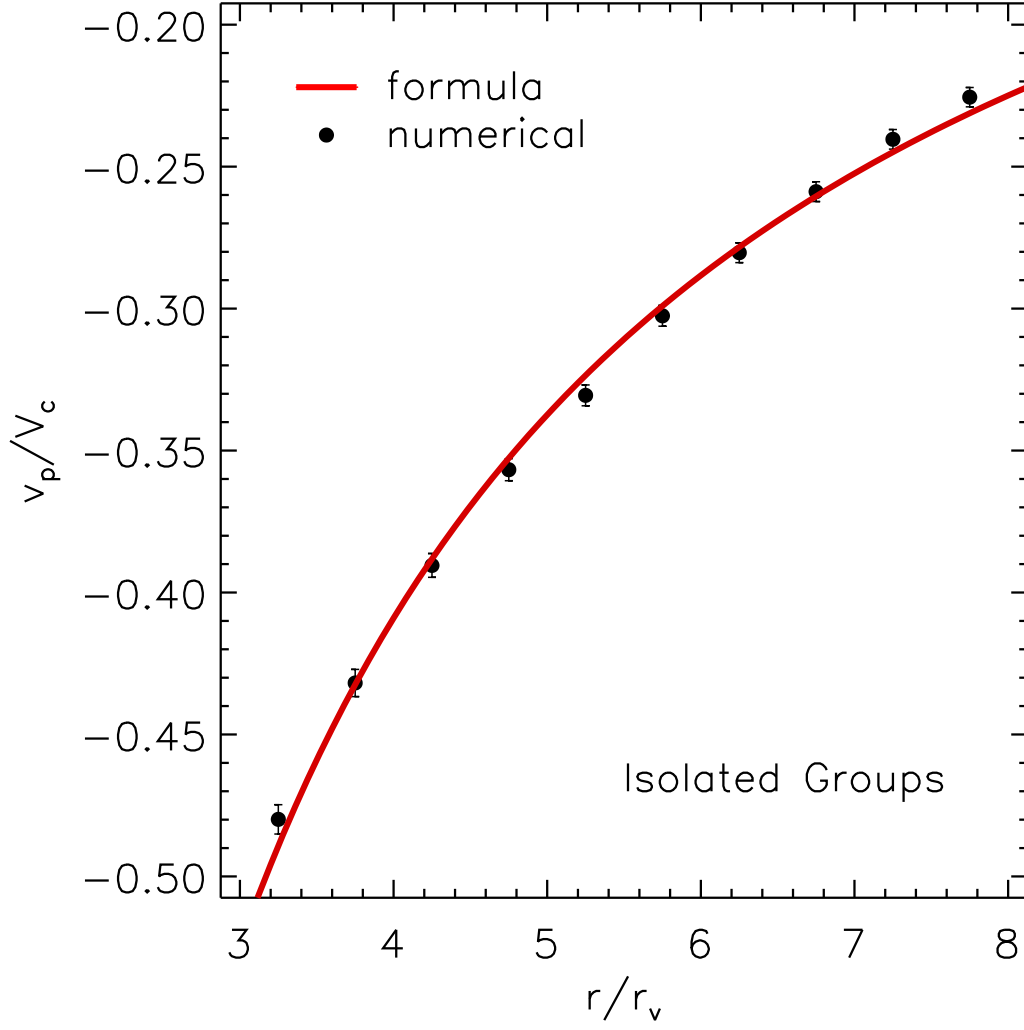


Fig. 6.— Same as Figure 1 but for the case of the isolated groups.

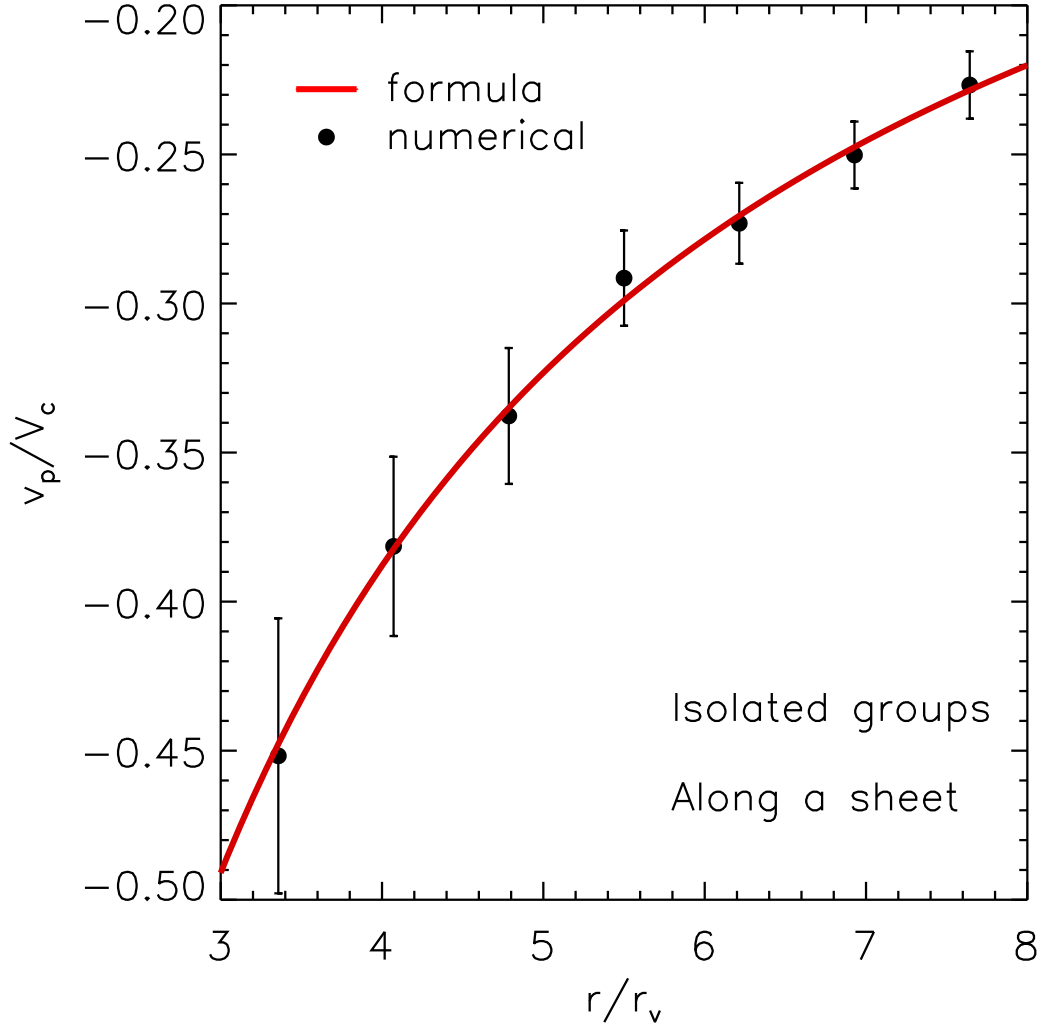


Fig. 7.— Same as Figure 3 but for the case of the isolated groups.

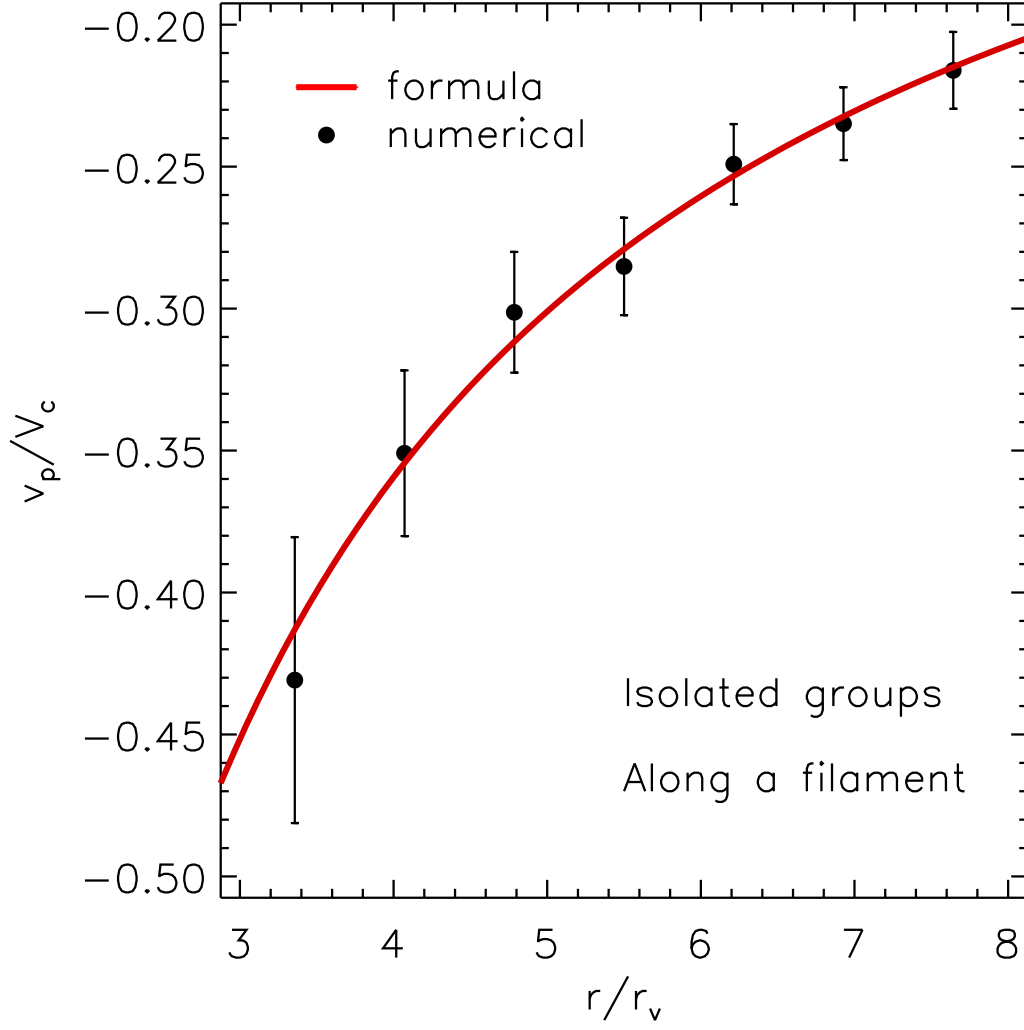


Fig. 8.— Same as Figure 4 but for the case of the isolated groups.

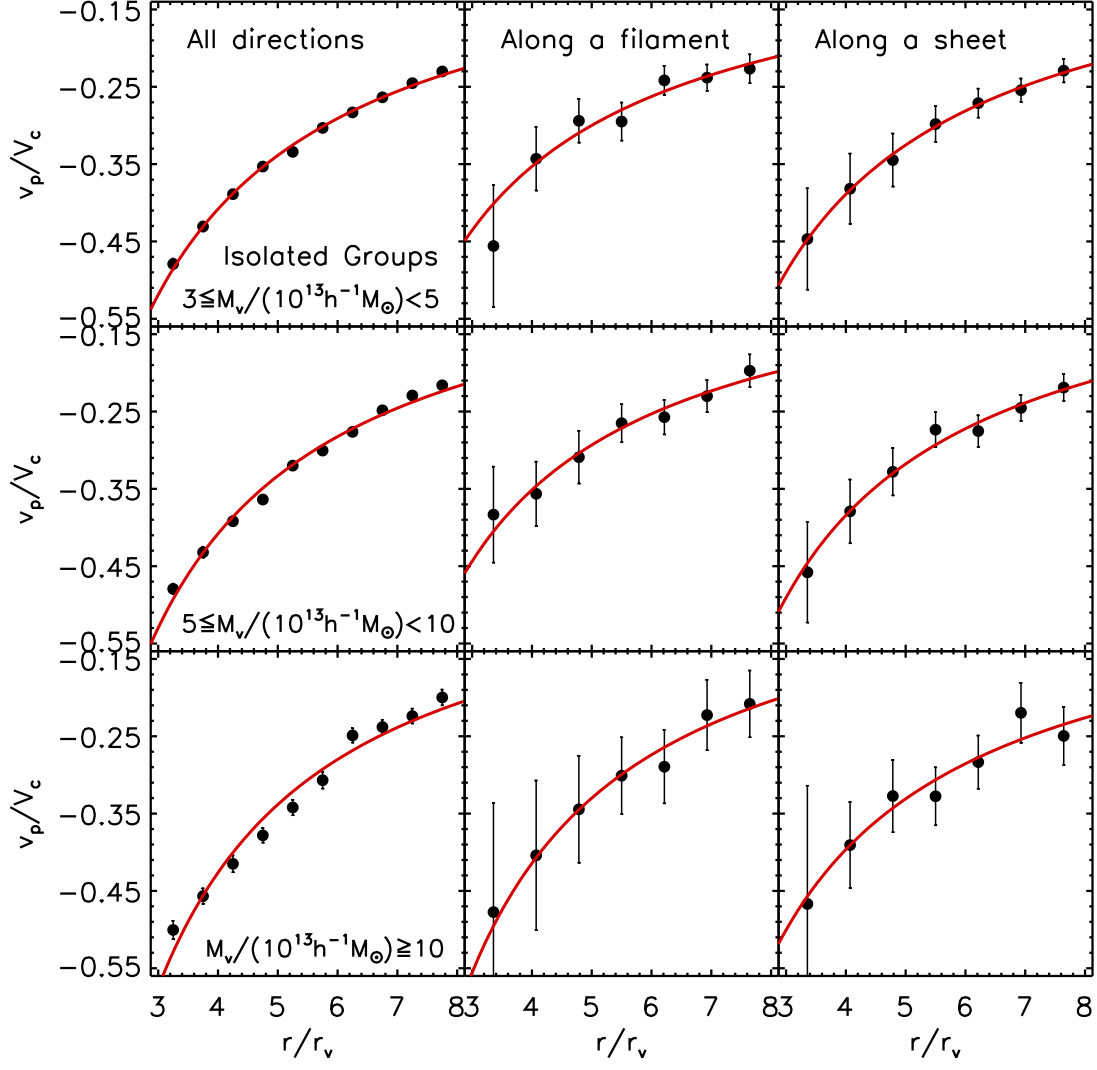


Fig. 9.— Same as Figure 5 but for the case of the isolated groups.

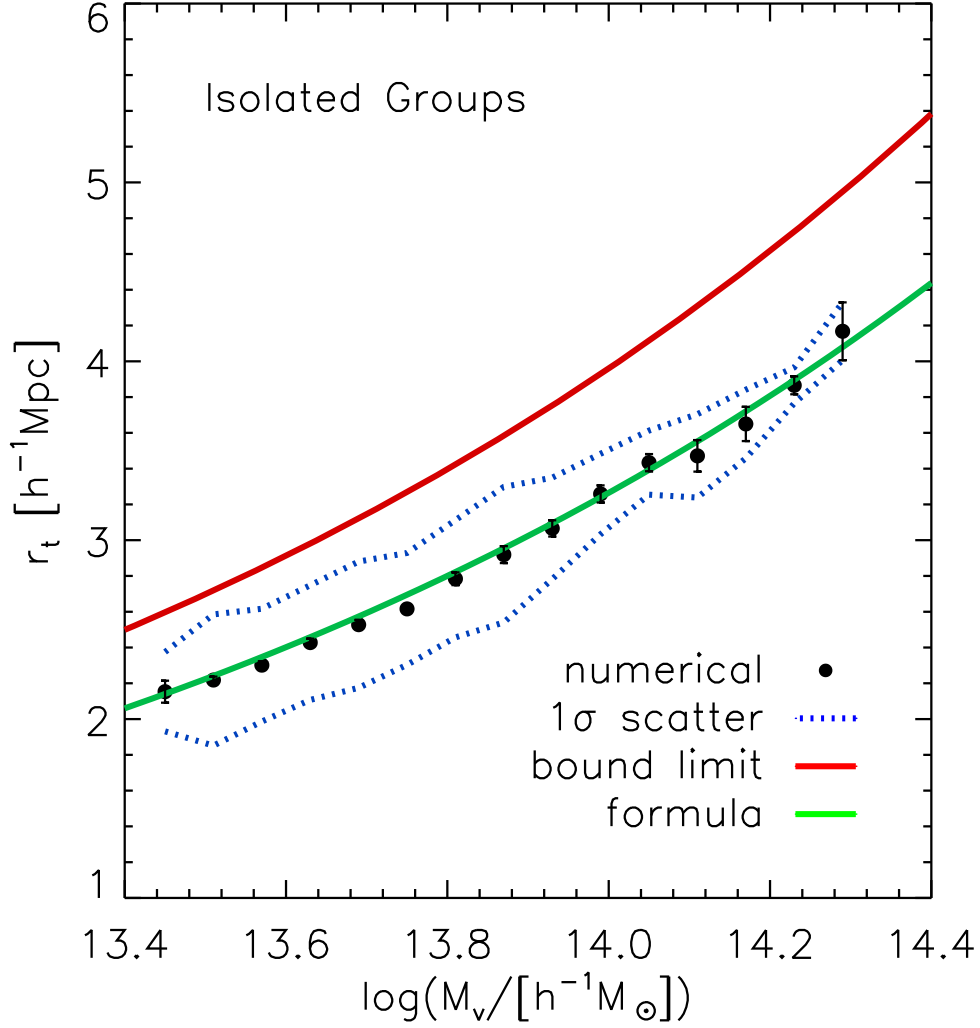


Fig. 10.— Average turn-around radius as a function of the virial mass of the isolated groups. The black filled circles represent the mean value of the turn-around radius averaged over the central groups at each mass bin, the dotted blue line represents the one standard deviation scatter around the average value, the solid green line represent the original formula derived by, and the red solid line represents the bound-limit predicted by the Planck cosmology.

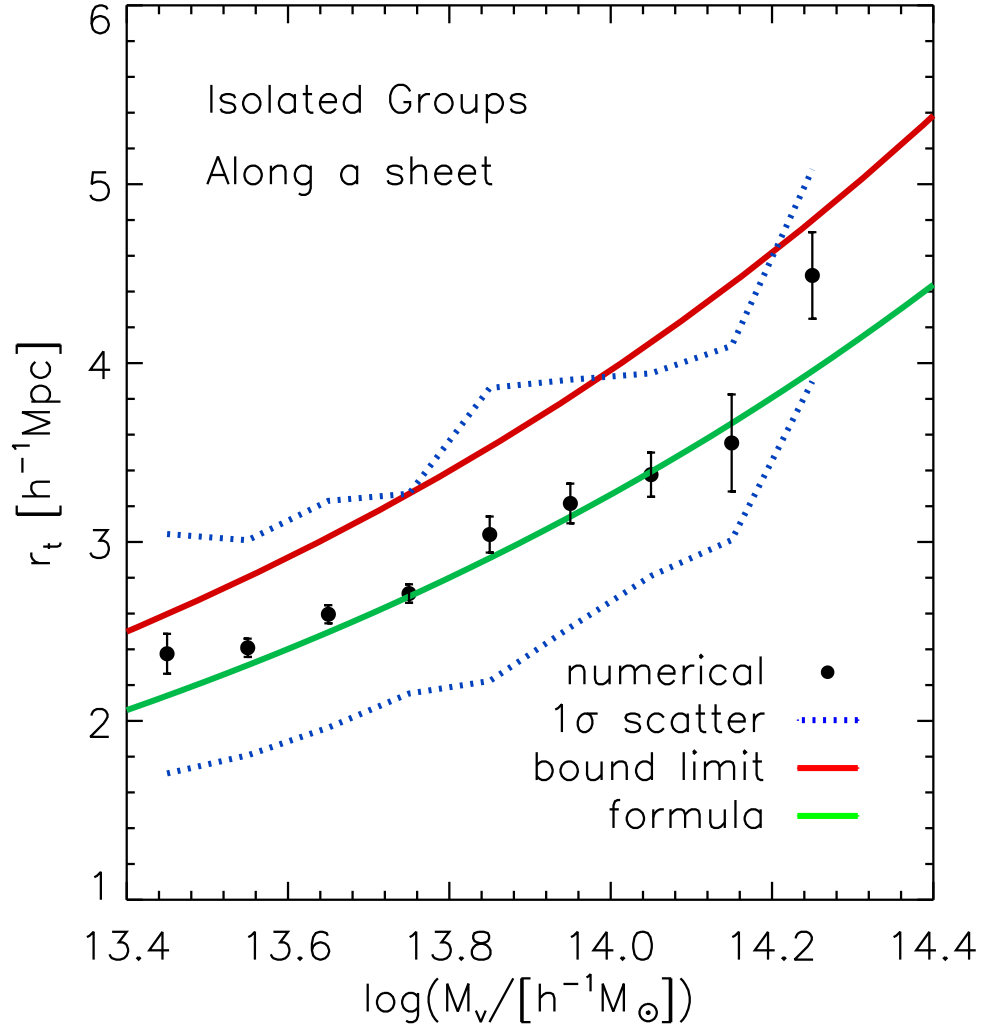


Fig. 11.— Same as Figure 10 but for the case of the bound-zone sheets.

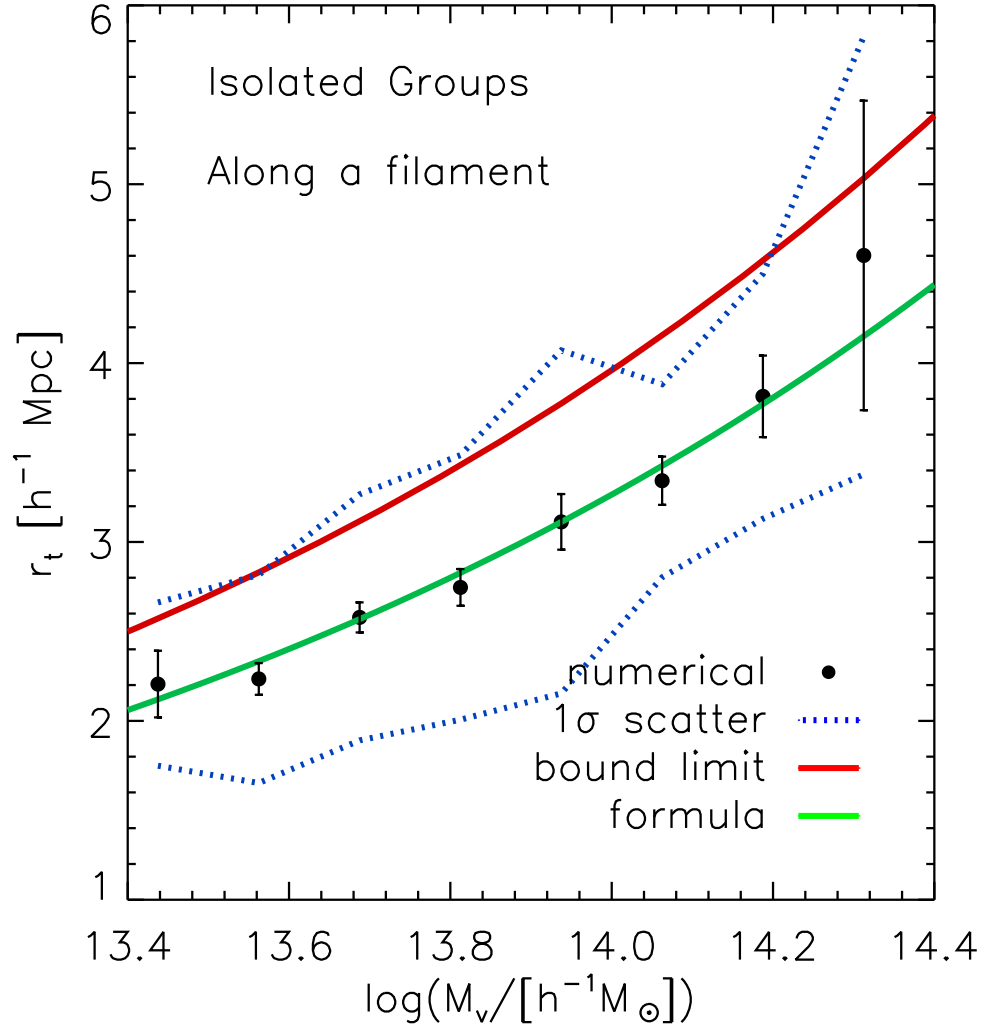


Fig. 12.— Same as Figure 10 but for the case of the bound-zone filaments.

Table 1. Mass range (M_v) and number (N_g) of the main groups, the direction along which the bound-zone peculiar velocity profile is reconstructed, the best-fit parameters of the analytic formula, a and b in Equation (2).

M_v ($10^{13}h^{-1} M_\odot$)	N_h	Direction	a	b
[3, 5)	3975	All	$0.68^{+0.01}_{-0.02}$	$0.26^{+0.01}_{-0.02}$
[3, 5)	3975	Sheet	0.59 ± 0.09	0.18 ± 0.10
[3, 5)	3975	Filament	0.58 ± 0.12	0.29 ± 0.14
[5, 10)	2842	All	$0.74^{+0.01}_{-0.02}$	$0.32^{+0.01}_{-0.02}$
[5, 10)	2842	Sheet	0.69 ± 0.09	0.29 ± 0.09
[5, 10)	2842	Filament	0.63 ± 0.12	0.33 ± 0.12
[10, ∞)	1659	All	0.88 ± 0.02	0.43 ± 0.01
[10, ∞)	1659	Sheet	0.79 ± 0.09	0.38 ± 0.08
[10, ∞)	1659	Filament	0.72 ± 0.11	0.46 ± 0.11

Table 2. Same as Table 1 but for the case of the isolated main groups.

M_v ($10^{13} h^{-1} M_\odot$)	N_h	Direction	a	b
[3, 5)	1088	All	1.30 ± 0.04	0.83 ± 0.02
[3, 5)	1088	Sheet	1.18 ± 0.34	0.80 ± 0.14
[3, 5)	1088	Filament	0.97 ± 0.33	0.73 ± 0.17
[5, 10)	407	All	1.44 ± 0.05	0.91 ± 0.02
[5, 10)	407	Sheet	1.25 ± 0.35	0.85 ± 0.14
[5, 10)	407	Filament	1.10 ± 0.37	0.81 ± 0.17
[10, ∞)	45	All	1.80 ± 0.10	1.04 ± 0.04
[10, ∞)	45	Sheet	1.22 ± 0.09	0.80 ± 0.30
[10, ∞)	45	Filament	1.70 ± 0.16	1.01 ± 0.35